STRUCTURAL TRANSFORMATION OF 2:1 DIOCTAHEDRAL LAYER SILICATES DURING DEHYDROXYLATION-REHYDROXYLATION REACTIONS

FABRICE MULLER, VICTOR DRITS,[1] ALAIN PLANÇON, AND JEAN-LOUIS ROBERT

ISTO, CNRS-University of Orléans, 1A rue de la Férollerie, 45071 Orléans, Cedex 2, France
[1] Geological Institute of the Russian Academy of Sciences, Pyzhevsky per.7, Moscow, Russia

Abstract—The structural transformation of dioctahedral 2:1 layer silicates (illite, montmorillonite, glauconite, and celadonite) during a dehydoxylation-rehydroxylation process has been studied by X-ray diffraction, thermal analysis, and infrared spectroscopy. The layers of the samples differ in the distribution of the octahedral cations over the *cis*- and *trans*-sites as determined by the analysis of the positions and intensities of the 11*l*, 02*l* reflections, and that of the relative displacements of adjacent layers along the *a* axis (*c* cos β/*a*), as well as by dehydroxylation-temperature values. One illite, glauconite, and celadonite consist of *trans*-vacant (*tv*) layers; Wyoming montmorillonite is composed of *cis*-vacant (*cv*) layers, whereas in the other illite sample *tv* and *cv* layers are interstratified. The results obtained show that the rehydroxylated Al-rich minerals (montmorillonite, illites) consist of *tv* layers whatever the distribution of octahedral cations over *cis*- and *trans*-sites in the original structure. The reason for this is that in the dehydroxylated state, both *tv* and *cv* layers are transformed into the same layer structure where the former *trans*-sites are vacant.

The dehydroxylation of glauconite and celadonite is accompanied by a migration of the octahedral cations from former *cis*-octahedra to empty *trans*-sites. The structural transformation of these minerals during rehydroxylation depends probably on their cation composition. The rehydroxylation of celadonite preserves the octahedral-cation distribution formed after dehydroxylation. Therefore, most 2:1 layers of celadonite that rehydroxylate (~75%) have *cis*-vacant octahedra and, only in a minor part of the layers, a reverse cation migration from former *trans*-sites to empty octahedra occurred. In contrast, for a glauconite sample with a high content in [IV]Al and [VI]Al the rehydroxylation is accompanied by the reverse cation migration and most of the 2:1 layers are transformed into *tv* layers.

Key Words—Cation Migration, Celadonite, *Cis*-Vacant Octahedra, Dehydroxylation, Glauconite, Illite, Rehydroxylation, Smectites, Structure, *Trans*-Vacant Octahedra.

INTRODUCTION

The study of clay minerals by thermal analysis has a long history during which a rich empirical material has been collected. Dioctahedral smectites and finely dispersed micas are characterized by a wide range of dehydroxylation temperatures (Brindley, 1976; Grim *et al.*, 1951; Grim, 1968; Guggenheim, 1990; Guggenheim and Koster van Gross, 1992; Heller-Kallai *et al.*, 1962; Koster van Gross and Guggenheim, 1987, 1990; Mackenzie, 1957, 1982; Tsipursky *et al.*, 1985). It is also remarkable that these dehydroxylated minerals can regain OH groups after heating in water vapor (Mackenzie, 1957; Grim, 1968).

The most reliable structural results have been obtained for aluminous minerals. Wardle and Brindley (1972) and Udagawa *et al.* (1974) determined the dehydroxylated structure for powdered pyrophyllite and muscovite. Pyrophyllite and muscovite consist of *trans*-vacant (*tv*) 2:1 layers. Their dehydroxylated structures are similar to their original form, but contain five-coordinated Al cations instead of six-coordinated ones.

Guggenheim *et al.* (1987), Koster van Gross and Guggenheim (1987, 1990), and Guggenheim (1990) used a detailed crystallo-chemical approach to consid-

er the dynamics of the dehydroxylation process of aluminous dioctahedral 2:1 layer silicates assuming that montmorillonites, beidellites, and illites have the same structure of 2:1 layers as pyrophyllite and muscovite. However, it has been found by oblique-texture electron diffraction and the simulation of X-ray diffraction (XRD) patterns that most montmorillonites as well as some illites and interstratified illite-smectites (I-S) are *cis*-vacant (*cv*) or have coexistence of *tv* and *cv* layers (Tsipursky and Drits, 1984; Zvyagin *et al.*, 1985; Drits *et al.*, 1996, 1998; Reynolds and Thompson, 1993; McCarty and Reynolds, 1995; Cuadros and Altaner, 1998). The derivative thermal gravimetric (DTG) curves of most montmorillonites have one endothermic peak near 700°C whereas beidellites and illites dehydroxylate near 550°C. I-S are often characterized by two endothermic reactions near 500 and 700°C (Mackenzie, 1957; Grim, 1968). In *cv* layers the OH-OH edge is not shared and thus OH-OH forms a common edge to occupied and vacant *cis*-octahedra. The OH-OH edge length is considerably longer than the length of the shared OH-OH edge of *tv* layers. Drits *et al.* (1995) assumed that thermal energy needed for a proton to jump to the nearest OH group to form a water molecule strongly depends on the distance be-

tween the nearest OH groups. Therefore *cv* montmo-rillonite requires a higher dehydroxylation energy than *tv* illite because of the longer OH-OH distance. These authors also showed that, contrary to *tv* layers, the dehydroxylation of *cv* aluminous 2:1 layers occurs in two stages. During the first stage the adjacent OH groups are replaced by a single residual oxygen atom, O_r, and the Al cations, which originally occupied *cis*- and *trans*-sites become, respectively, five- and six-co-ordinated. During the second stage, the Al cations mi-grate from the former *trans*-sites to vacant pentagonal prisms. As a result, the dehydroxylated structures of the former *cv* and *tv* aluminous layers are similar.

Concerning the dehydroxylation of Fe^{3+}-rich dioc-tahedral 2:1 phyllosilicates (glauconites, celadonites, and nontronites), there are two contradictory interpre-tations. Heller-Kallai and Rozenson (1980) and Roz-enson and Heller-Kallai (1980) concluded that there is no cation migration during dehydroxylation whatever the cation composition. They assumed that in Fe^{3+}-rich 2:1 phyllosilicates, Fe^{3+} occupies both *cis*- and *trans*-octahedra. However, the structural study of nontroni-tes, glauconites, and celadonites by diffraction meth-ods has shown that these minerals always consist of *tv* 2:1 layers (Tsipursky and Drits, 1984, Sakharov *et al.*, 1990, Drits *et al.*, 1997, Manceau *et al.*, 2000). In addition, Tsipursky *et al.* (1985) showed that octahe-dral cations migrate from *cis*- to *trans*-sites in the de-hydroxylated Fe^{3+}-rich dioctahedral 2:1 layer silicates, assuming that, as in the case of the aluminous varie-ties, O_r locates midway between two closest Fe^{3+} with the same *z* coordinate. As a result, Fe^{3+} cations, which formerly occupied the *cis*-sites, become six-coordinat-ed after migration. Muller *et al.* (2000) studied the dehydroxylation process of several Fe-rich minerals using XRD. The diffraction patterns were simulated using the CALCIPOW computer program designed for the simulation of the intensities diffracted by layer structures containing different kinds of layers and stacking faults (Plançon, 1981). Several models were calculated, differing by the site occupancies and lo-cation of residual oxygen anions. An occupancy of the former vacant *trans*-sites and the location of the resid-ual oxygens in one of the two possible positions of the former OH groups yields the best fit between ex-perimental and calculated patterns, confirming the mi-gration of Fe^{3+} cations for the dehydroxylated cela-donites and glauconites. The Fe^{3+} cations in the former *trans*- and *cis*-sites preserve their five-coordination and the location of the residual anions provides struc-tural stability for glauconite and celadonite dehydrox-ylates.

In contrast to the study of dehydroxylation reac-tions, there are only a few studies devoted to the re-hydration of dehydroxylated dioctahedral 2:1 phyllos-ilicates having different original structure and com-position (Mackenzie, 1957; Grim, 1968; Emmerich *et*

al., 1999). Montmorillonites with an endothermic peak near 700°C can regain their initial hydroxyls by cool-ing in the presence of water vapor. However, the DTG curves of these rehydroxylated montmorillonites have either one peak near 600°C or two peaks near 500 and 650°C, respectively. Dehydroxylated beidellites and il-lites can also be rehydroxylated. In this case, the loss of hydroxyls of the rehydroxylated samples in DTG analysis occurs at temperatures near the dehydroxy-lation temperature of the original samples. An expla-nation to the difference in thermal behavior of rehy-droxylated montmorillonites and rehydroxylated bei-dellites and illites was proposed by Drits *et al.* (1995) where they suggested that original *cv* montmorillonites can be transformed into *tv* rehydroxylates. This hy-pothesis was confirmed experimentally for smectites (Emmerich *et al.*, 1999), but not for illites. The struc-ture of rehydroxylated Fe-rich dioctahedral 2:1 layer silicates has not been examined.

In this paper, XRD, DTG analysis, and infrared (IR) spectroscopy was used to study natural (N), dehydrox-ylated (D), rehydoxylated (R), and de-rehydroxylated (DR) dioctahedral 2:1 clay minerals consisting of *tv* and *cv* or interstratified *tv/cv* layers of different cation compositions. The fundamental method for the study of the polymorphous transformation of *cv* layers into *tv* layers (or *vice versa*) is XRD. Thermal gravimetric (TG) analysis and IR were used to complement the interpretation of the XRD data.

EXPERIMENTAL

Two illites (identified below as *tv* and *cv/tv*), a Wy-oming montmorillonite, a glauconite, and a celadonite were studied. Structural formulae and references where these samples are described are presented in Table 1.

Powder XRD patterns were recorded using $MoK\alpha$ radiation with an INEL CPS 120 diffractometer equipped with a curved position-sensitive detector. This detector permits a simultaneous recording of the XRD pattern in a 2θ interval from 6 to 30°. The sample holder was a Lindemann glass tube with a 1-mm di-ameter. The diffusion background arising from the empty tube was subtracted in the experimental XRD patterns.

The unit-cell parameters were determined by using the following procedure. The values of *b* were deter-mined by measuring *d*(060) values. For mica samples, the positions of 003 reflections permitted the deter-mination of the *d*(001) = *c* sin β values, whereas the $11\bar{2}$ and 112 reflections were used to estimate *a* and β using well-known relationships between *hkl* indices, *d*(*hkl*), and the monoclinic unit-cell parameters (Sak-harov *et al.*, 1990; Muller *et al.*, 2000). This procedure provides an accurate determination of the *a* and β pa-rameters if the sample consists of identical 2:1 layers (either *tv* and *cv*). The interstratification of *cv* and *tv*

Table 1. Structural formula of samples under study calculated per $O_{10}(OH)_2$.

		Illite[1] (sample 60)	cv/tv illite[2]	Wyoming montmorillonite[3]	Glauconite[4] (sample 6869)	Celadonite[5] (sample 69)
Tetrahedral cations	Si	3.63	3.47	3.96	3.78	3.94
	Al	0.37	0.53	0.04	0.22	0.06
Octahedral cations	Al	1.41	1.71	1.53	0.55	0.05
	Fe^{3+}	0.10	0.04	0.18	0.89	1.15
	Fe^{2+}	0.07	—		0.18	0.36
	Mg	0.42	0.26	0.26	0.39	0.41
	Ti	—	0.01	0.01	—	
Interlayer cations	K	0.77	0.63		0.80	0.83
	Na	0.07	0.07	0.35	—	0.01
	Ca	0.01	0.07		—	0.03

[1] Ivanovskaya *et al.* (1989).
[2] Horton (1983).
[c] Private communication of R. Glaeser.
[4,5] Drits *et al.* (1997).

layers induces a displacement of the 11*l* reflections from the positions corresponding to periodic *tv* and *cv* dioctahedral micas, in which case the *a* and β values determined by this procedure do not correspond to the actual parameters. The criteria described by Drits and McCarty (1996) which use experimental $d(11l)$, $d(00l)$, $d(060)$, and calculated *c* cos β/*a* values have been applied to distinguish *cv*, *tv,* and interstratified *cv/tv* mica structures. Errors in determination of the $d(hkl)$ values do not exceed 0.002 Å.

The natural samples were heated to 650°C (glauconite and celadonite) or 750°C (illites and montmorillonite) for dehydroxylation. The heating rate was 100°C/h, each sample remaining heated at the upper temperature for 1 h, and then cooled in air. To rehydroxylate samples, gold capsules were filled with the dehydroxylate plus 20 wt % water. The capsules were placed in a Tuttle-type pressure vessel at 400°C and 1 kbar for 10 d. After removal from the pressure vessel, the rehydroxylated samples were heated at 120°C for several hours to dry the sample.

Thermal gravimetric analyses were performed with a Setaram TGA 92 microanalyser, with a heating rate of 10°C/min. A 30-mg sample was used for each measurement. The derivatives of the TG curves (DTG) compare the weight loss, which was assigned to water evolved from hydroxyl groups.

IR spectra in the OH-stretching region were obtained with a Perkin Elmer Paragon 1000PC spectrometer. A 3-mg sample (except for glauconite: 0.5 mg) was mixed with 150 mg of KBr in a steel capsule (0.5 mg only for *cv/tv* illite). The disk obtained after pressing was heated at 140°C for 15 h to remove most of the absorbed water. The transmitted intensities were recorded from 3000 to 4000 cm^{-1} at 1-cm^{-1} intervals.

RESULTS

Figure 1 shows the XRD patterns obtained for the four states (N, D, R, DR) of the five studied samples. Table 2 provides the unit-cell parameters of these sam-

ples and the *c* cos β/*a* value which characterizes the relative displacement of the adjacent layers along the *a* axis. Wyoming montmorillonite has a turbostratic structure. Therefore, the determination of its unit-cell parameters is limited to $d(001)$ and *b*; *a* is taken as *b*/$\sqrt{3}$. Figure 2 compares the TG and DTG curves of the original and rehydroxylated samples. Figure 3 shows the IR spectra of the original and rehydroxylated samples in the stretching-vibration region. The wavenumbers corresponding to the centers of the complex OH-stretching bands are shown at each transmittance minimum.

tv illite (sample 60)

The XRD patterns and unit-cell parameters (Figure 1a; Table 2) of the N and R specimens reflect the diffraction and structural characteristics of dioctahedral *tv* 1*M* mica, *i.e.,* strong 11$\bar{1}$, 11$\bar{2}$, and 112 reflections, almost zero intensity of the 111 reflection, and relative displacements of adjacent layers along the *a* axis between −0.39 and −0.40 (Bailey, 1984; Drits *et al.,* 1984a, 1993). The XRD patterns for the D and DR forms are quite similar and preserve the main diffraction features of the N and R samples (Table 2). Thus, the XRD data show that there is no octahedral-cation migration. In all states the *trans*-octahedral sites remain vacant.

This conclusion is consistent with the DTG curve (Figure 2a). The shift in peaks of the maximum water lost in N (600°C) and R (575°C) is probably related to a partial decrease in the particle size after dehydroxylation. The IR spectra of the N and R specimens are very similar (Figure 3a). The center of the OH-stretching band of N (3606 cm^{-1}) shifts to higher frequencies for R (3621 cm^{-1}).

cv/tv illite

This sample, described by Horton (1983) as 3*T* illite, was found among clay minerals associated with a hydrothermal ore vein. Reynolds and Thompson
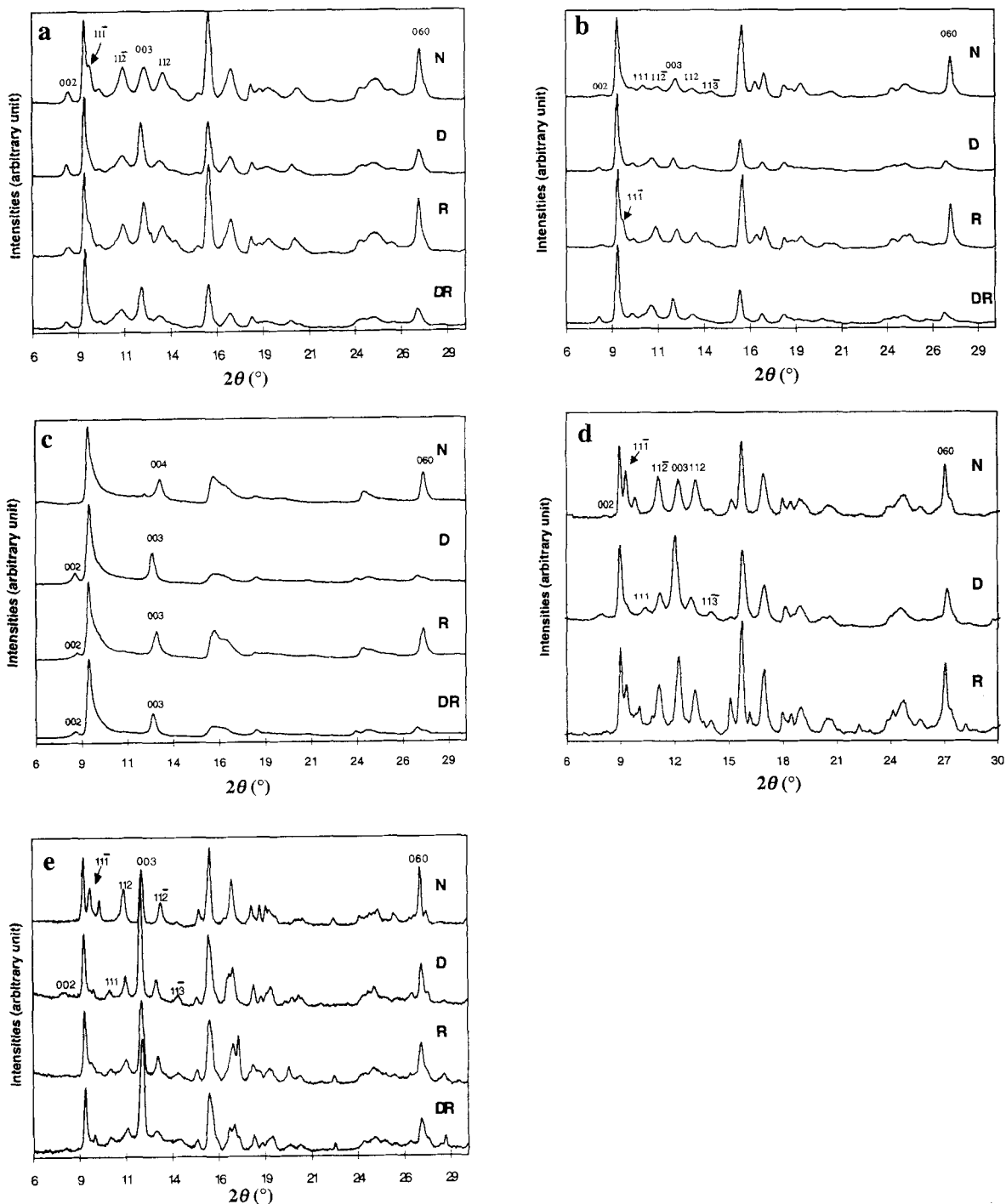
Figure 1.   XRD patterns ($\lambda K\alpha Mo$ = 0.70926 Å) of a) illite 60, b) cv/tv illite, c) Wyoming montmorillonite, d) glauconite 6869, and e) celadonite 69 in natural (N), dehydroxylated (D), and rehydroxylated (R) states. XRD patterns of illite 60, cv/tv illite, Wyoming montmorillonite, and celadonite 69 are also presented in de-rehydroxylated (DR) state.

(1993) and Drits *et al.* (1993) showed that the XRD patterns of dioctahedral tv $3T$ and cv $1M$ mica polytypes are very similar. Because, for the studied sample, $d(060)$ = 1.501 Å, and the minimum periodicity along the c^* axis is 9.966 Å, the hexagonal unit-cell parameters of the $3T$ polytype should be $a = b/\sqrt{3} = 6d(060)/\sqrt{3} = 5.200$ Å, $c = 3d(001) = 29.899$ Å, and $\gamma = 120°$. After indexing and determination of the d

Table 2.   Unit-cell parameters and $c\cos \beta/a$ values of samples under study.

Sample	State	a (Å)	b (Å)	c (Å)	β (°)	$c\cos \beta/a$	$d(001)$ (Å)
Illite (sample 60)	N	5.238	9.018	10.14	101.48	−0.385	9.933
	D	5.265	9.024	10.24	100.98	−0.374	10.050
	R	5.252	9.042	10.16	101.46	−0.387	9.956
	DR	5.291	9.048	10.26	101.22	−0.382	10.065
cv/tv illite	N	5.214	9.006	10.12	99.97	−0.337	9.966
	D	5.299	9.108	10.34	102.11	−0.413	10.110
	R	5.265	9.018	10.17	101.52	−0.390	9.966
	DR	5.352	9.120	10.33	102.31	−0.418	10.090
Wyoming montmorillonite	N	5.193	8.994	—	—	—	12.560
	D	5.241	9.078	—	—	—	9.708
	R	5.196	9.000	—	—	—	9.558
	DR	5.252	9.096	—	—	—	9.681
Glauconite (sample 6869)	N	5.270	9.090	10.19	101.28	−0.378	9.993
	D	5.242	9.054	10.23	99.25	−0.314	10.098
	R	5.271	9.096	10.17	100.69	−0.358	9.996
Celadonite (sample 69)	N	5.220	9.060	10.22	100.92	−0.371	10.062
	D	5.233	9.030	10.21	98.78	−0.299	10.089
	R	5.235	9.060	10.26	99.24	−0.315	10.128
	DR	5.240	9.036	10.17	98.55	−0.290	10.062
Average error		± 0.005 Å	± 0.006 Å	± 0.02 Å	± 0.05		

values of the 3*T* unit cell, the differences between the calculated spacings, d_{calc}, and experimental values, d_{exp}, of the 101, 102, 104, and 105 reflections vary from 0.004 to 0.009 Å. These differences are higher than the error of the measurement of the *d* values. Hence, the 3*T*-polytype designation must be discarded. Indexing of the experimental XRD pattern based on a one-layer monoclinic unit cell, with $a = 5.214$ Å, $b = 9.006$ Å, $c = 10.12$ Å, and $\beta = 99.97°$, provides the best agreement between the experimental and calculated $d(02l, 11l)$; the difference between d_{calc} and d_{exp} does not exceed 0.002 Å. Note that the *b* parameter of the unit cell is not equal to $a\sqrt{3}$, as it must for the 3*T* unit cell. One of the main differences between *tv* 3*T* and *cv* 1*M* polytypes is the $c\cos \beta/a$ value which is −0.333 for *tv* 3*T* (transformed into a one layer monoclinic unit-cell) and −0.300 for aluminous *cv* 1*M* polytypes (Drits *et al.,* 1993). The $c\cos \beta/a$ value calculated for the monoclinic unit cell (−0.337) of the studied sample is close to that of the 3*T* polytype which has been discounted. The most reliable interpretation of the diffraction features is that the sample is composed of randomly interstratified *tv* and *cv* 2:1 layers with relative proportions near 0.4 and 0.6 as determined by the method proposed by Drits and McCarty (1996) using the experimental $d(11l)$ values. Such an interpretation is confirmed below by DTG.

The positions and intensities of the 11*l* and 02*l* reflections in the XRD pattern of the D specimen are typical of dehydroxylated *tv* 1*M* illites (Figure 1b)

with a $c\cos \beta/a$ value (−0.413, Table 2) which significantly differs from $c\cos \beta/a = -0.337$ as determined for the N specimen. The modification of the XRD pattern of the D specimen in comparison to that of the N pattern confirms a predominance of *cv* 2:1 layers in the N structure. The XRD patterns of N and D *tv*-illites and muscovites are quite similar because the dehydroxylation of *tv* 2:1 aluminous layers is not accompanied by an octahedral-cation migration (Guggenheim *et al.,* 1987, 1990; Drits *et al.,* 1995). In contrast, the XRD patterns of N and D *cv* illite should be substantially different owing to the migration of the Al cations from former *trans*-octahedra into empty *cis*-prisms (Drits *et al.,* 1995). An illite sample consisting of *cv* and *tv* layers is then expected to show the *tv* characteristics in the D state, as is the case for this sample.

The XRD pattern of the R specimen is typical of a *tv* 1*M* illite (Figure 1b; Table 2). As expected, the dehydroxylation of the rehydroxylate reproduces the main diffraction features of the D specimen (Figure 1b). This conclusion agrees with the thermal effects (Figure 2b). The DTG curve of the N sample contains two maxima: the weaker at 550°C and the stronger at 700°C. These maxima respectively correspond to the dehydroxylation of *tv* and *cv* 2:1 layers (Drits *et al.,* 1995, 1998). The DTG curve of the rehydroxylate contains only one maximum at 550°C, which confirms the existence of only one type of layer in the rehydroxylated sample. This result indicates also the trans-

→

Figure 2.   TG and DTG curves of a) illite 60, b) *cv/tv* illite, c) Wyoming montmorillonite, d) glauconite 6869, and e) celadonite 69 in natural (thin line) and rehydroxylated (thick line) states.
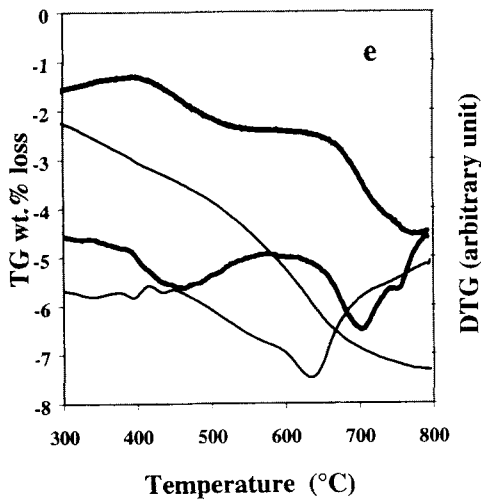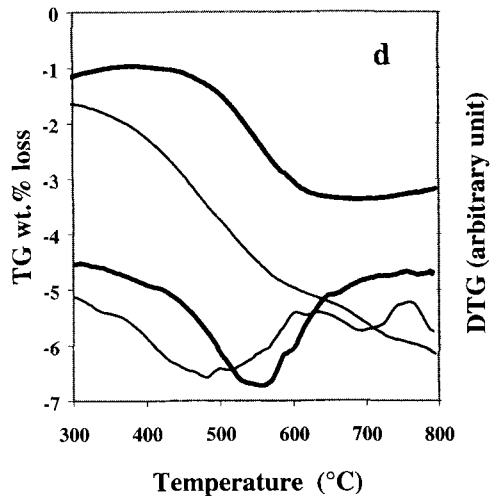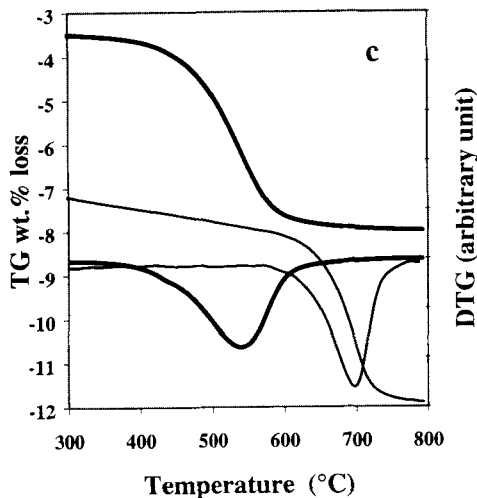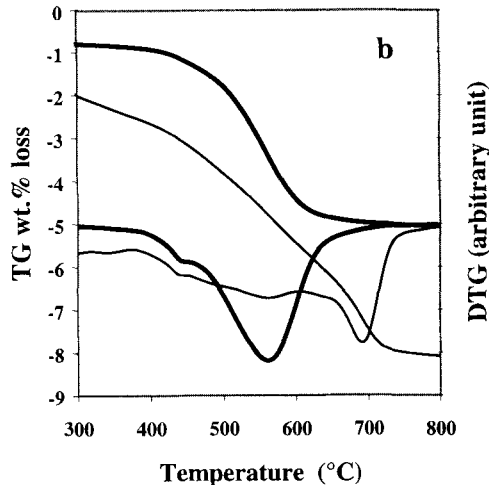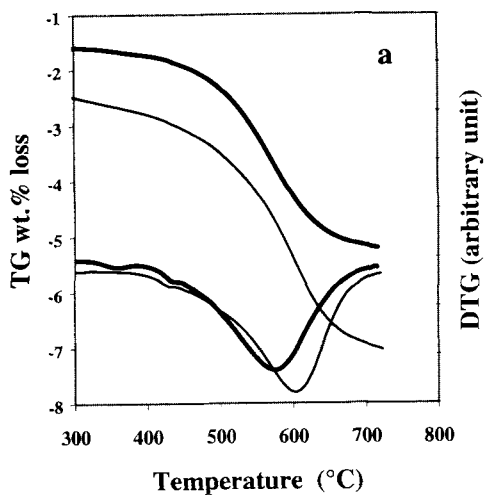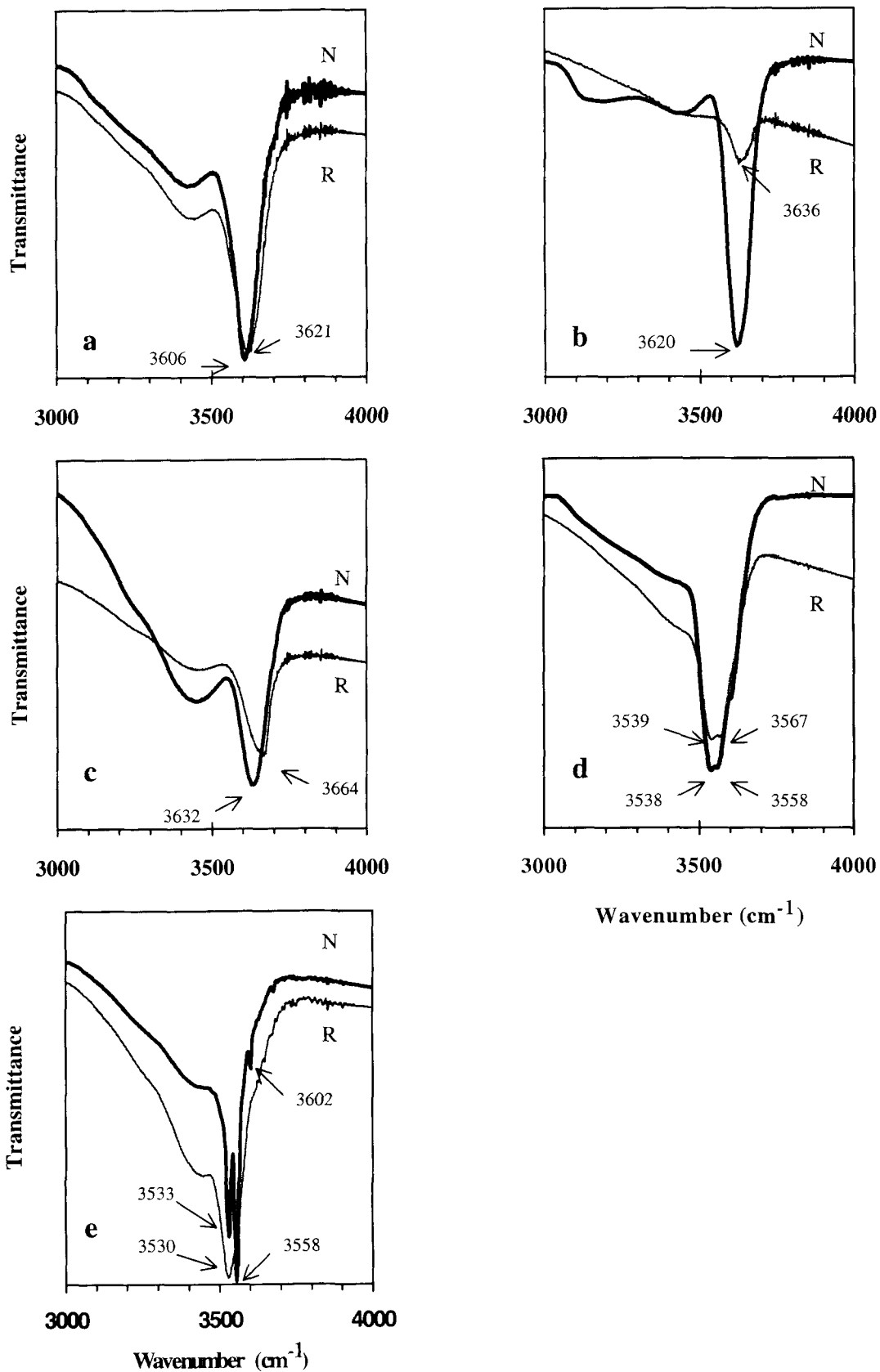
formation of *cv* into *tv* layers during dehydroxylation. The comparison of the IR spectra of the original and rehydroxylated specimens shows that rehydroxylation is accompanied by a significant decrease of the OH band and a displacement of its center from 3620 to 3636 cm^{-1} (Figure 3b).

Wyoming montmorillonite

The turbostratic stacking of the sample makes it impossible to determine the octahedral cation distribution over the *trans*- and *cis*-octahedra using XRD. However, it is noted that the XRD patterns of the N and R specimens are quite similar (Figure 1c), except for 00*l* reflections. The N specimen of Figure 1c is in its natural state [$d(001) = 12.56$ Å] and the R sample is in a dried state [$d(001) = 9.55$ Å, Table 2]. The structure of the 2:1 layers of the N and R specimens can be deduced from the DTG curves (Figure 2c). The DTG curve of the N sample contains one strong maximum at 700°C. This maximum corresponds to the dehydroxylation of *cv* layers (Drits *et al.*, 1995). In contrast, the dehydroxylation of the R specimen occurs at a lower temperature (540°C) which corresponds to the dehydroxylation of *tv* layers. Thus, the thermal effects show that the dehydroxylation-rehydroxylation process of the Wyoming montmorillonite induces the transformation of *cv* to *tv* layers. As for the *tv* illite and the *cv/tv* illite described previously, the main intensity band in the IR spectrum of the rehydroxylate shifts to a higher value compared to that of the original specimen from 3632 to 3664 cm^{-1}.

Glauconite (sample 6869)

The main diffraction features of the sample in its N, D, and R states (Figure 1d) show that dehydroxylation is accompanied by a migration of octahedral cations from *cis*- into *trans*-sites. For the D specimen, the rather weak 111, 11$\bar{2}$, 112, and 11$\bar{3}$ maxima typical for *cv* 1*M* dioctahedral micas replace the strong 11$\bar{1}$, 11$\bar{2}$, and 112 reflections observed for the N specimen, and typical of *tv* 1*M* dioctahedral micas (Figure 1d). A significant decrease in the relative displacement of adjacent layers from -0.378 for the N specimen to -0.314 for the D sample confirms that cation migration occurs. Drits *et al.* (1997) showed that the *c* cos β/*a* value of dioctahedral 1*M* micas depends on their chemical composition. The higher the content of octahedral Fe^{2+} and Mg, the lower the |*c* cos β/*a*| value. For this reason, the |*c* cos β/*a*| value for the N specimen is lower than the values of *tv* 1*M* illites. According to the procedure described by Drits *et al.* (1984a), a transformation of *tv* 1*M* to *cv* 1*M* dioctahedral mica

with the chemical composition of sample 6869 should change the *c* cos β/*a* values from -0.378 to -0.311. The latter is close to the -0.314 value determined for the D specimen (Table 2). The XRD patterns of the N and R specimens are quite similar with respect to the reflection-intensity distribution. This indicates that the rehydroxylation process is accompanied by a reverse cation migration. However, the |*c* cos β/*a*| value for the R specimen (-0.358) is significantly lower than that (-0.378) for the N specimen. According to Drits and McCarty (1996), the R specimen should contain 25–30% of *cv* 2:1 layers based on this value. Thus, after rehydroxylation, most layers have *trans*-vacant octahedra. As a side effect, the dehydroxylation-rehydroxylation process slightly disturbs the structure, with the characteristic appearance of a slight increase in background at the 02*l* and 11*l* reflections.

Note that the IR spectra of the N and R specimens in the stretching vibration region are quite similar (Figure 3d), with two bands located near 3538 and 3558 cm^{-1} for the N specimen, and near 3539 and 3567 cm^{-1} for the R specimen. The DTG patterns of the N and R samples have a broad maximum at 480 and 560°C, respectively. The small dehydroxylation peak at 700°C probably corresponds to a carbonate impurity.

Celadonite (sample 69)

The XRD patterns for the N and D specimens of the celadonite and glauconite samples are quite similar (Figure 1d and 1e). This shows that the dehydroxylation of both minerals is accompanied by an octahedral-cation migration from *cis* into former *trans*-sites. A significant decrease of |*c* cos β/*a*| from 0.371 for the N specimen of celadonite to 0.299 for the D specimen confirms this conclusion. The value of |*c* cos β/*a*| = 0.371 for the N specimen is related to a high content of Mg and Fe^{3+}, as for the glauconite sample. The similarity of the XRD patterns for the D and R specimens (Figure 1e) shows that their 2:1 layers have a near identical cation distribution. Also, their *c* cos β/*a* values are similar (-0.299 *vs.* -0.315). If the relative displacement of adjacent *cv* layers in dioctahedral micas having a celadonite composition is -0.299 or -0.290 as found in the D and DR specimens, respectively (Table 2), then, according to Drits and McCarty (1996), the R specimen should contain 25–30% of *tv* 2:1 layers. Then, after rehydroxylation, there is no reverse cation migration from former *trans*- to empty *cis*-octahedra for most of the layers. In this respect, the structural transformation of the dehydroxylated celadonite and glauconite samples during the rehy-

←

Figure 3.   IR spectra in the OH-stretching region of a) illite 60, b) *cv/tv* illite, c) Wyoming montmorillonite, d) glauconite 6869, and e) celadonite 69 in natural (N) and rehydroxylated (R) states.

droxylation process differs substantially. A small reverse cation migration occurs in celadonite whereas considerable reverse cation migration occurs in glauconite. The dehydroxylation of the R specimen of celadonite is not accompanied by significant cation migration ($c \cos \beta /a = -0.290$, Table 2), and the former *trans*-sites remain occupied.

The DTG curves of the celadonite sample (Figure 2e) agree with the transformations described above. The DTG curve of the original sample (Figure 2e) can be described by two peaks near 550 and 650°C, which cannot be assigned, respectively, to *tv* and *cv* layers because XDR shows unambiguously that the sample contains only *tv* layers. A water loss showing two peaks has been observed in pyrophyllite and muscovite by Guggenheim (1990), and in illite-smectites by Drits *et al.* (1998). Guggenheim (1990) explained this effect by the change of coordination of the Al next-nearest neighbors of the OH pairs during dehydroxylation. In celadonite, the existence, within the layers, of domains differing in the octahedral cation distribution (Drits *et al.*, 1997), can also induce a heterogenous loss of water. The maximum water lost at 650°C is significantly higher than that observed for *tv* Al-rich dioctahedral 2:1 layer silicates. Drits *et al.* (1998) showed that for the Al-rich *cv* and *tv* layers, the dehydroxylation temperatures (T_d) are, respectively, below and above 600°C. Two factors can be responsible for a higher value of T_d for celadonites. First, according to crystal structure refinements (Zvyagin, 1967; Drits *et al.*, 1984b), octahedral sheets of celadonite 2:1 layers are significantly thicker than sheets of illites. The thicker the octahedral sheet, the longer the OH-OH shared edges. More thermal energy is then required for dehydroxylation. Second, a local compensation of the negative charge of the residual oxygen atoms in a mica dehydroxylate is more difficult to occur if these oxygen atoms are coordinated by divalent cations. Therefore, it is likely that the greater the amount of divalent octahedral cations in 2:1 layers, the greater the resistance of these layers to be transformed and the higher the thermal energy required for the layer dehydroxylation. The DTG curve of the R specimen has a maximum water loss at 700°C (Figure 2e). This increase of T_d in comparison with that of the original sample confirms a presence of *cv* 2:1 layers in the rehydroxylated structure. The maximum in water loss observed at 450°C in the DTG curve of the rehydroxylate corresponds to the dehydroxylation of *tv* 2:1 layers.

Figure 3e shows that the well resolved IR spectrum of the original sample is replaced by a single wide OH band at 3530 cm⁻¹. The "center of gravity" of the OH band in the R sample shifts to a lower frequency in comparison with that in the N specimen (Figure 3). This is the opposite behavior of the studied Al-rich samples.

DISCUSSION

The data obtained by TGA and IR spectroscopy confirm that the experimental rehydroxylation process produces hydroxylation of the samples. The results obtained here show that the structural features of dehydroxylated and rehydroxylated dioctahedral 2:1 layer silicates depend on their chemical composition as well as on the original distribution of octahedral cations over *cis*- and *trans*-sites. Dioctahedral 2:1 phyllosilicates in their initial state can be subdivided into three main groups: Al-rich *tv*, Al-rich *cv*, and Fe^{3+}, Mg-rich ($^{VI}Fe^{3+}$, $^{VI}Mg > ^{VI}Al$) *tv* 2:1 minerals. Rehydroxylated dioctahedral 2:1 layer silicates are subdivided into two groups. The first group consists of rehydroxylated Al-rich minerals, which are composed of *tv* layers regardless of the distribution of the octahedral cations over *cis*- and *trans*-sites in the original structures. The second group is represented by the Fe^{3+}, Mg-rich minerals for which *tv* 2:1 layers are transformed into *cv* ones during dehydroxylation, and preserve this structure partially after rehydroxylation. Table 3 summarizes the main structural transformations of the studied samples during dehydroxylation and rehydroxylation reactions. To trace the structural transformations of dioctahedral 2:1 layer silicates during the dehydroxylation-rehydroxylation reactions, it is useful to consider the causes of the structural transitions within each subgroup.

Trans-vacant illites

As mentioned above, the cation distribution in the octahedral sheet in the dehydroxylated state of these minerals is the same as that in the natural state. No cation migration occurs. These cations become five-coordinated, the residual oxygen atoms O_r being located at the same z coordinate as octahedral cations and midway between them. We assume that a structural rearrangement takes place in reverse order during the rehydroxylation process: water molecules migrate into the sample and react with the residual oxygen atom according to $H_2O + O_r \rightarrow 2(OH)$. This reaction reconstructs the octahedral coordination of the Al cations bonded to the newly formed OH groups. Thus, the original structural arrangement of the 2:1 layers is recovered. However, as shown in Table 2, the transition from the N to R state of sample 60 leads to a noticeable increase of the *a* and *b* unit-cell parameters. This effect is unexpected. It is obvious that dehydroxylation alone cannot change the valency of the octahedral cations present in sample 60 (mainly Al and Mg, Table 1). *Cis*-octahedral cation occupancy and composition should also be the same in the N and R specimens.

Cis-vacant and cv/tv illite and smectites

The structural transitions of the octahedral sheet of an original Al-rich *cv* 2:1 layer to its D and R states

Table 3. The main structural transformations of the studied samples after dehydroxylation and rehydroxylation reactions.

Sample	Status		
	N	D	R
Illite (sample 60)	*tv* layers	no cation migration, five-fold coordination of Al and Mg cations, location of a residual oxygen atom, O_r, midway between two closest Al, Mg cations.	no cation migration, reconstruction of *tv* layers due to the reaction $O_r + H_2O \rightarrow 2(OH)$.
cv/tv illite	*cv/tv*	migration of the cations into vacant *cis*-sites in *cv* layers and formation of a structure similar to that of dehydroxylated *tv* illites.	no cation migration, all layers are *tv*, as in the previous case.
Wyoming montmorillonite	*cv*	migration of octahedral cations into vacant *cis*-sites and formation of a structure similar to that of dehydroxylated *tv* illites.	no cation migration, all layers are *tv*.
Glauconite (sample 6869)	*tv*	migration of octahedral cations into vacant former *trans*-sites, location of a residual oxygen atom, O_r, in one of two possible positions of OH groups.	partial reverse cation migration from former *trans*-sites into empty *cis*-sites and formation of 70–75% *tv* layers. No cation migration in the remaining 25–30% of layers which are *cv*.
Celadonite (sample 69)	*tv*	migration of octahedral cations into vacant former *trans*-sites, location of a residual oxygen atom, O_r, in one of two possible positions of OH groups.	there is no cation migration in most layers, but ~20–30% of them have been transformed into *tv* layers owing to the cation migration.

are shown schematically in Figure 4. As seen in Figure 4a, each of the two adjacent OH groups form non-shared edges which are considerably longer than shared OH-OH edges in *tv* layers. For the latter, the OH groups screen the electrostatic repulsion between octahedral cations. For *tv* layers, the dehydroxylation of *cv* layers is accompanied by the replacement of two adjacent OH groups by a residual oxygen atom. The Al cations that originally occupied *cis*- and *trans*-sites become five- and six-coordinated, respectively (Figure 4b). The structure of the dehydroxylated 2:1 layers is unstable because the bond lengths between the six-coordinated Al cations and the oxygen atoms are unrealistically long relative to unheated structures. Drits *et al.* (1995) showed that no shift of octahedral cations or anions can provide an appropriate charge saturation of the oxygen atoms of the octahedral polyhedron. Structural stabilization is obtained by the migration of the Al cations from the former *trans*-sites to the empty five-coordinated prisms. The resulting structure (Figure 4c) is identical to that of the *tv* dehydroxylates where the Al cations provide homogeneous local-charge compensation. During rehydroxylation these heat-treated layers remain as *tv* layers (Figure 4d).

The XRD data, as well as the DTG curves, obtained for *cv/tv* illite and Wyoming smectite are consistent with this model. The difference in the OH-OH lengths in the original *cv* layer (Figure 4a) and rehydroxylated *tv* layer (Figure 4d) explains the significant decrease in dehydroxylation temperatures for the R specimens of *cv/tv* illite and Wyoming montmorillonite (Figure

2b and 2c) as proposed by Drits *et al.* (1995). An explanation based on an energy rise required for octahedral-cation migration is discarded. Dehydroxylation induces cation migration in layers of glauconite and celadonite. Nevertheless, Figure 2d and 2e shows that dehydroxylation temperatures are lower for the N samples.

The transition from N to D as well as from the R to DR states of *cv/tv* illite leads to a significant increase of *a*, *b*, and *c* unit-cell parameters (Table 2). Drits *et al.* (1995) noted that the main reason for the increase of the *b* parameters for dehydroxylated Al-rich 2:1 layers is a tendency for octahedral cations to move away from each other along the *b* axis to increase the Al-O_r distance to an appropriate equilibrium value. The observed decrease of these parameters in the rehydroxylates compared to those in the dehydroxylated specimens (Table 2) is a direct consequence of the replacement of the residual oxygen atom by two OH groups, which reconstructs an octahedral coordination for cations and provides cation-anion bond lengths appropriate for this coordination, and with lower *a* and *b* parameters. Rehydroxylation reconstructs the original 9.966-Å periodicity along the *c** axis (Table 2). The significant increase of the *d*(001) value for the D and DR specimens may be the result of trapping H_2O molecules within the interlayers which leave the structure during dehydroxylation. The transformation of *cv* layers to *tv* layers in Wyoming montmorillonite has a negligible influence on the unit-cell parameters (Table 2). A similar negligible effect

may also be the case for all dioctahedral Al-rich smectites; *cv* and *tv* 2:1 layers of identical octahedral cation composition should have identical or nearly identical unit-cell lateral dimensions.

Fe³⁺-rich dioctahedral tv 2:1 layer silicates

The structural transformations in celadonites and glauconites from the original to the dehydrated state and then to the rehydroxylated state are shown schematically in Figure 5. As previously, it might be assumed that during dehydroxylation, adjacent OH groups are replaced by a residual O_r oxygen atom. The O_r atom locates midway between and at the same z-coordinate level as the octahedral cations, and occupied octahedra are transformed into five-coordinated prisms (Figure 5b). In such cases, the octahedral cation-O_r distance will become $b/6$, *i.e.*, 1.51–1.52 Å, and this distance is too short for cations with pentagonal coordination. Therefore, the octahedral cations must move away from each other, as observed in dehydroxylated muscovite where the Al-O_r distance is 1.69 Å (Udagawa *et al.*, 1974). According to Drits *et al.* (1995), such a rearrangement of the Al and O_r atoms is the main reason for the larger *a* and *b* parameters compared to the original values. The cations Fe^{2+}, Mg, and Fe^{3+} are relatively large in comparison with Al^{3+}. Thus the replacement of Al by Fe and Mg should increase the cation-O_r distance and increase the *b* parameter in a way that is not compatible with the limited lateral expansion of the tetrahedral sheets. Tsipursky *et al.* (1985) argued that this factor is responsible for the cation migration from *cis*- to *trans*-sites. The main reason for this assumption was that cation migration is absent in glauconites where the content of ^{VI}(Fe + Mg) is lower or equal to the ^{VI}Al content. However, Muller *et al.* (2000) showed by simulation of XRD patterns, that for Fe-rich dioctahedral layer silicates [^{VI}(Fe + Mg) ≥ ^{VI}Al]], O_r atoms in the D structure are located in former OH positions, eliminating the problem of the short Fe, Mg-O_r distances. Figure 5c shows a model where the O_r atoms occupy one of the two former hydroxyl sites distributed along the [100] direction with a period equal to the *a* parameter; Fe, Mg cations have five-coordination and are located in the former *cis*-sites. Figure 5d shows an arrangement for the dehydroxylated octahedral sheet, assuming an additional cation migration from *cis*- to *trans*-sites, in comparison with Figure 5c. These two structural models (Figure 5c and 5d), having different cation distributions, are characterized by different stability fields, which can be estimated by using the Pauling electrostatic valency principle. In both models the residual anions are strongly undersaturated with respect to positive charge because they receive this charge only from two five-coordinated cations. The degree of undersaturation may be decreased by a shortening of the cation-residual anion bonds because the shorter the bond
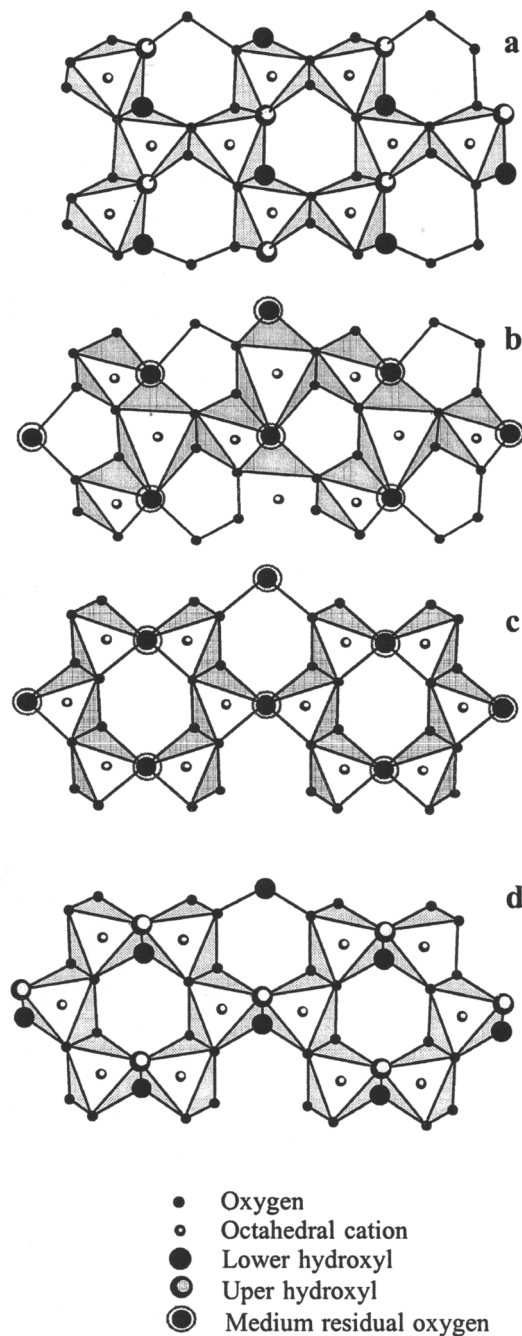

●   Oxygen
○   Octahedral cation
⬤   Lower hydroxyl
◉   Uper hydroxyl
◎   Medium residual oxygen

Figure 4. Schematical representation of octahedral sheet during the dehydroxylation-rehydroxylation reaction of Al-rich *cv* 2:1 layers silicates. Natural state (a), dehydroxylation (b), cations migration (c), and rehydroxylated *tv* state (d).

length, the greater the bond strength, *i.e.*, the higher the saturation of the anion by positive charge. Because cation repulsion should be screened by anions, note that in the *trans*-vacant dehydroxylate model (Figure 5c) the smaller cation to O_r distances must greatly increase cation-cation repulsion. These repulsions occur

Oxygen
Octahedral cation
Lower hydroxyl or residual oxygen
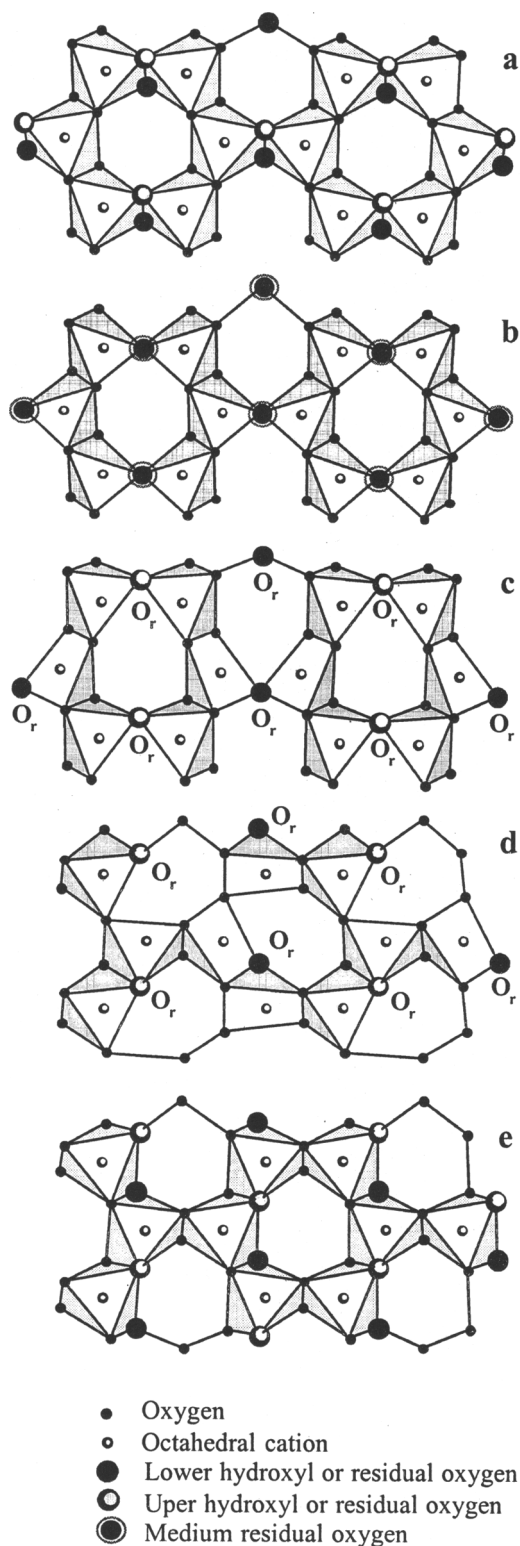Uper hydroxyl or residual oxygen
Medium residual oxygen

Figure 5. Schematical representation of octahedral sheet during the dehydroxylation-rehydroxylation reaction of Fe-rich *tv* 2:1 layers silicates. Natural state (a), dehydroxylation (c), cations migration (d), and rehydroxylated *cv* state (e). The

because only one O_r anion provides the required screening of repulsions caused by each of the two nearest cations along the *b* axis (Figure 5c). In addition, the O_r anion is not at the same *z* level as the cations. In contrast, in the dehydroxylate *cis*-vacant model (Figure 5d), the repulsion of cations bonded to the O_r anion is screened by shortened anion edges, which occurs also in non-heated dioctahedral 2:1 layers. Thus, the octahedral-cation migration and location of the residual oxygen atoms in the former OH sites stabilize the dehydroxylate structure of celadonites and glauconites. The migration of octahedral cations from *cis*- to *trans*-sites was observed in these dehydroxylated minerals by Tsipursky *et al.* (1985). The former *tv* layers are transformed into layers with vacant five-fold prisms formed from the former *cis*-octahedra. The observed decrease of *b* for dehydroxylated samples 69 and 6869 is in accordance with cation migration (Table 2). The values of *c* cos β/*a* for the original and de-hydroxylate samples also agrees with the location of Fe, Mg cations in the sites as described above.

Figure 5e illustrates the rehydroxylation process with the replacement of each O_r anion by two OH groups in *cv* 2:1 layers. The positions and intensity of *hkl* reflections in the XRD patterns of rehydroxylated celadonite (Figure 1e) as well as the unit-cell parameters and the mutual disposition of adjacent layers (Tables 2) are consistent with the model described. Note that after rehydroxylation a portion of the dehydroxylated layers (25–30%) in the celadonite sample returns to a *tv* sheet. A more complex transformation takes place for the glauconite sample. For dehydroxylated glauconite, rehydroxylation of the 2:1 layers is accompanied by reverse cation migration from the former *trans*-sites into empty prisms and the replacement of O_r anions by pairs of OH groups. As a result, the glauconite rehydroxylate consists of the interstratification of 70–75% *tv* and 25–30% *cv* layers. This effect may be related to partial heterogeneity in the cation composition of individual 2:1 layers in the original samples. During rehydroxylation, the layers with a higher Al content are transformed into *tv* layers whereas layers with a lower Al content preserve the cation distribution of the dehydroxylate. Probably, the reverse migration of octahedral Al cations to vacant *cis*-sites of R layers provides a more stable configuration.

←

situation for (b) corresponds to the model of Al-rich *tv* 2:1 layer silicates where the residual oxygen atoms move to the same *z* coordinate as the octahedral cations.

REFERENCES

Bailey, S.W. (1984) Crystal chemistry of the true micas. In *Micas, Reviews in Mineralogy, Volume 13*, S.W. Bailey, ed., Mineralogical Society of America, Washington, D.C., 13–60.

Brindley, G.W. (1976) Thermal transformations of clays and layer silicates. In *Proceedings of International Clay Conference, 1975*, J. Fripiat, ed., Applied Publishing Ltd., Wilmette, Illinois, USA, 119–129.

Cuadros J. and Altaner S.P. (1998) Composition and structural features of the octahedral sheet in mixed-layer illite/smectite from bentonites. *European Journal of Mineralogy, 10*, 111–124.

Drits, V.A. and McCarty, D.K. (1996) The nature of diffraction effects from illite-smectite consisting of interstratified trans-vacant and cis-vacant 2:1 layers: A semiquantitative technique for determination of layer-type content. *American Mineralogist, 81*, 852–863.

Drits, V.A., Plançon, A., Sakharov, B.A., Besson, G., Tsipursky, S.I., and Tchoubar, C. (1984a) Diffraction effects calculated for structural models of K-saturated montmorillonite containing different types of defects. *Clay Minerals, 19*, 541–562.

Drits, V.A., Tsipursky, S.I., and Plançon, A. (1984b) Application of the method for the calculation of intensity distribution to electron diffraction structural analysis. *Izvestiya Akademii Nauk S.S.S.R., Seriya Physica, 2*, 1708–1713. (in Russian).

Drits, V.A., Weber, F., Salyn, A.L., and Tsipursky, S.I. (1993) X-ray identification of one-layer illite varieties: Application to the study of illite around uranium deposits of Canada. *Clays and Clay Minerals, 41*, 389–398.

Drits, V.A., Besson, G., and Muller, F. (1995) An improved model for structural transformations of heat-treated aluminous dioctahedra 2:1 layer silicates. *Clays and Clay Minerals, 43*, 718–731.

Drits, V.A., Salyn, A.L., and Sucha, V. (1996) Structural transformation of illite-smectite from Dolva Ves hydrothermal deposite: Dynamics and mechanisms. *Clays and Clay Minerals, 44*, 181–196.

Drits, V.A., Dainyak, L.G., Muller, F., Besson, G., and Manceau, A. (1997) Isomorphous cation distribution in celadonites, glauconites and Fe-illites determined by infrared, Mössbauer and EXAFS spectroscopies. *Clay Minerals, 32*, 153–179.

Drits, V.A., Lindgreen, H., Salyn, A.L., Ylagan, R., and McCarty, D.K. (1998) Semiquantitative determination of *trans*-vacant and *cis*-vacant 2:1 layers in illites and illite-smectites by thermal anlysis and X-ray diffraction. *American Mineralogist, 83*, 1188–1198.

Emmerich, K., Thule Madsen, F., and Kahr, G. (1999) Dehydroxylation behavior of heat-treated and steam-treated homoionic *cis*-vacant montmorillonites. *Clays and Clay Minerals, 47*, 591–604.

Grim, R.E. (1968) *Clay Mineralogy: International Series in the Earth and Planetary Sciences*. McGraw-Hill Book Company, New York, 596 pp.

Grim, R.E., Bradley, W.F., and Brown, G. (1951) *X-ray Identification and Crystal Structures of Clay Minerals*, G.W. Brindley, ed., Mineralogical Society, London, 138–172.

Guggenheim, S. (1990) The dynamics of thermal decomposition in aluminous dioctahedral 2:1 layer silicates: A crystal chemical model. In *Proceedings of 9th International Clay Conference, Volume 2*, V.C. Farmer and Y. Tardy, eds., Strasbourg, France, 99–107.

Guggenheim, S. and Koster van Groos, A.F. (1992) High-pressure differential thermal analysis (HP-DTA). II. Dehydroxylation reactions at elevated pressures in phyllosilicates. *Journal of Thermal Analysis, 38*, 2529–2548.

Guggenheim, S., Chang, H.Y., and Koster van Groos, A.F. (1987) Muscovite dehydroxylation: High-temperature studies. *American Mineralogist, 72*, 537–550.

Heller-Kallai, L. and Rozenson, I. (1980) Dehydroxylation of dioctahedral phyllosilicates. *Clays and Clay Minerals, 28*, 355–368.

Heller-Kallai, L., Farmer, V.C., Mackenzie, R.C., Mitchell, B.D., and Taylor, H.F.W. (1962) The dehydroxylation and rehydroxylation of triphormic dioctahedral clay minerals. *Clay Minerals Bulletin, 5*, 56–72.

Horton, D. (1983) Argilitic alteration. Association with the amethyst vein system. Ph.D. thesis, University of Illinois, Urbana-Champaign, Illinois, USA.

Ivanovskaya, T.A., Tsipursky, S.I., and Yakovleva, O.V. (1989) Mineralogy of globular glauconites from Vendian and Rephean of the Ural and Siberia. *Litologiya Poleznye Iskopaemye, 3*, 83–89. (in Russian).

Koster van Groos, A.F. and Guggenheim, S. (1987) High-pressure differential thermal analysis (HP-DTA) of the dehydroxylation of Na-rich montmorillonite and K-exchanged montmorillonite. *American Mineralogist, 72*, 1170–1175.

Koster van Groos, A.F. and Guggenheim, S. (1990) Dehydroxylation of Ca- and Mg-exchanged montmorillonite. *American Mineralogist, 74*, 627–636.

Mackenzie, R.C. (1957) *The Differential Thermal Investigation of Clays*. Mineralogical Society, London, 456 pp.

Mackenzie, R.C. (1982) *Down-to-Earth Thermal Analysis: Thermal Analysis*. Wiley Heyden Ltd., Chichester, Great Britain, 25–36.

Manceau, A., Lanson, B., Drits, V.A., Chategner, D., Gates, W.P., Wu, J., Huo, D., and Stucki, J.W. (2000) Oxidation-reduction mechanism of iron in dioctahedral smectites: 1. Crystal chemistry of oxidized reference nontronite. *American Mineralogist, 85*, 133–152.

McCarty, D. and Reynolds, R.C. (1995) Rotationally disordered illite-smectites in Paleozoic K-bentonites. *Clays and Clay Minerals, 43*, 271–284.

Muller, F., Drits, V.A., Besson, G. and Plançon, A. (2000) Dehydroxylation of Fe^{3+}, Mg-rich dioctahedral micas. (I) Structural transformation. *Clay Minerals, 35*, 491–504.

Plançon, A. (1981) Diffraction by layer structures containing different kinds of layers and stacking faults. *Journal of Applied Crystallography, 14*, 300–304.

Reynolds, R.C. and Thompson, C.H. (1993) Illite from the Postdam Sandstone of New York, a probable noncentrosymmetric mica structure. *Clays and Clay Minerals, 41*, 66–72.

Rozenson, J. and Heller-Kallai, L. (1980) Order-disorder phenomena accompanying the dehydroxylation of dioctahedral phyllosilicates. *Clays and Clay Minerals, 28*, 391–392.

Sakharov, B.A., Besson, G., Drits, V.A., Kameneva, M.Y., Salyn, A.N., and Smoliar, B.B. (1990) X-ray study of the nature of stacking faults in the structure of glauconites. *Clay Minerals, 25*, 419–435.

Tsipursky, S.I. and Drits, V.A. (1984) The distribution of octahedral cations in the 2:1 layers of dioctahedral smectites studied by oblique texture electron diffraction. *Clay Minerals, 19*, 177–192.

Tsipursky, S.I., Kameneva, M.Y., and Drits, V.A. (1985) Structural transformation of Fe^{3+}-containing 2:1 dioctahedral phyllosilicates in the course of dehydroxylation. In *Proceedings of the 5th Conference of the European Clay Groups*, J. Konta, ed., Prague, 569–577.

Udagawa, S., Urabe, K., and Hasu, H. (1974) The crystal structure of muscovite dehydroxylate. *Japanese Association for Mineralogy, Petrology and Geology,* **69,** 381–389.

Wardle, R. and Brindley, G.W. (1972) The crystal structures of pyrophyllite-1Tc and of its dehydroxylate. *American Mineralogist,* **57,** 732–750.

Zvyagin, B.B. (1967) *Electron Diffraction Analysis of Clay Mineral Structures.* Plenum Press, New York, 320 pp.

Zvyagin, B.B., Rabotnov, V.T., Sidorenko, O.V., and Kotelnikov, D.D. (1985) Unique mica consisting of noncentrosymmetric layers. *Izvestiya Akademii Nauk S.S.S.R., Seriya Geologiya,* **35,** 121–124. (in Russian).

E-mail of corresponding author: Fabrice.Muller@univ-orleans.fr